Adhesion and Merging of Lipid Bilayers: A Method for Measuring the Free Energy of Adhesion and Hemifusion

Yen Sun, Chang-Chun Lee, and Huey W. Huang*
Department of Physics and Astronomy, Rice University, Houston, Texas

ABSTRACT Lipid bilayers can be induced to adhere to each other by molecular mediators, and, depending on the lipid composition, such adhesion can lead to merging of the contacting monolayers in a process known as hemifusion. Such bilayer-bilayer reactions have never been systematically studied. In the course of our studies of membrane-active molecules, we encountered such reactions. We believe that they need to be understood whenever bilayer-bilayer interactions take place, such as during membrane fusion. For illustration, we discuss three examples: spontaneous adhesion between phospholipid bilayers induced by low pH, polymer-induced osmotic depletion attraction between lipid bilayers, and anionic lipid bilayers cross-bridged by multicationic peptides. Our purpose here is to describe a general method for studying such interactions. We used giant unilamellar vesicles, each of which was aspirated in a micropipette so that we could monitor the tension of the membrane and the membrane area changes during the bilayer-bilayer interaction. We devised a general method for measuring the free energy of adhesion or hemifusion. The results show that the energies of adhesion or hemifusion of lipid bilayers could vary over 2 orders of magnitude from -1 to -50×10^{-5} J/m^2 in these examples alone. Our method can be used to measure the energy of transition in each step of lipid transformation during membrane fusion. This is relevant for current research on membrane fusion, which focuses on how fusion proteins induce lipid transformations.

INTRODUCTION

Some fundamental interactions between lipid bilayers are well known and have been extensively studied, including van der Waals interactions (1,2), electrostatic double-layer forces (2), short-range repulsive hydration forces (3), and undulation-induced steric repulsion (4). These interactions involve the forces between two (flexible) surfaces. However, other interactions can occur between lipid bilayers because these bilayers possess internal degrees of freedom, including the possibility of redistribution of lipid components (5,6). Such interactions are induced by molecular mediators and result in either adhesion or partial merging between bilayers. In studies of membrane fusion, this partial merging (i.e., merging of the contacting leaflets but not the distal leaflets) is called hemifusion (7–12). In the course of our studies with various membrane-active molecules, we have encountered several examples of adhesion and hemifusion. We believe that such reactions can be important for membrane fusion. They could also distort the results of nonfusion vesicle experiments if the possible vesicle-vesicle reactions are not understood. Our purpose here is to use examples to illustrate mediator-induced bilayer-bilayer interactions and, of more importance, to describe methods for characterizing such interactions. In particular, we have devised a general method for measuring the free energy of adhesion or hemifusion. One possible application of this method is to analyze the multistep lipid transformations during membrane fusion. Potentially, the method can be used to determine the energy of transition for each step.

In the first example, we discovered a phenomenon of spontaneous adhesion between phospholipid bilayers induced by low pH. Examples of viral fusion proteins activated by low pH are well known (13,14). Much less known is the pH dependence of bilayer properties (15). In the second example, we injected a small amount of polyethylene glycol (PEG) solution between two bilayers, which induced an attraction between them and resulted in the development of a temporary contact zone. This osmotic depletion attraction between two surfaces is understood (2,16). Interestingly, for some lipid compositions, this process led to hemifusion at low pH (7–12). In the third example, the mediator of bilayer interaction is the multicationic peptide HIV-1 TAT48-60 (TAT). TAT is a prototype cell-penetrating peptide (17–19). Recently, it was suggested that TAT enters cells by causing leaky fusion of liposomes (20). When we injected a small amount of TAT solution between two anionic lipid bilayers, the bilayers developed a cross-bridged contact zone. As in the case of PEG, for some lipid compositions the contact zone led to hemifusion. The implications of these findings will be explored further in future experiments. Here, we concentrate on the methodology used to characterize these mediator-induced bilayer interactions.

We used two different methods to measure the adhesion energies depending on the strength of the interaction. To measure weak adhesion energies, we used the experimental method developed by Evans and co-workers (1,16,21–24), in which one flaccid giant unilamellar vesicle (GUV) is released to adhere to one tensed GUV. For strong adhesion

Submitted November 12, 2010, and accepted for publication January 10, 2011.

*Correspondence: hwhuang@rice.edu

Editor: Claudia Steinem.

0006-3495/11/02/0987/9 $2.00

doi: 10.1016/j.bpj.2011.01.013

including hemifusion, we positioned two tensed GUVs next to each other. We then injected a small amount of mediators toward the GUVs. The induced interactions were sufficiently strong that a contact zone developed between two tensed GUVs. We introduced a general method of data analysis to obtain the free energy of adhesion. The method is based on the variation principle of equilibrium state, and thus is independent of how the adhesion or hemifusion state is reached. The same principle applies to both weak and strong interactions.

MATERIALS AND METHODS

Materials

We purchased 1-stearoyl-2-oleoyl-*sn*-glycero-3-phosphocholine (SOPC); 1-stearoyl-2-oleoyl-*sn*-glycero-3-phosphoethanolamine (SOPE); 1,2-dioleoyl-*sn*-glycero-3-phosphocholine (DOPC); 1,2-dioleoyl-sn-glycero-3-phosphoethanolamine (DOPE); 1,2-di-(9Z-octadecenoyl)-*sn*-glycero-3-phospho-(1′-*rac*-glycerol) (DOPG); 1,2-dioleoyl-*sn*-glycero-3-phosphoethanolamine-N-(lissamine rhodamine B sulfonyl) (Rh-DOPE); 1-oleoyl-2-[12-[(7-nitro-2-1,3-benzoxadiazol-4-yl)amino]lauroyl]-*sn*-glycero-3-phosphocholine (NBD-PC); and cholesterol from Avanti Polar Lipids (Alabaster, AL). HIV-1 TAT48-60 (acetyl-GRKKRRQRRRPPQ-amide) was custom synthesized and purified to >95% HPLC by GenScript (Piscataway, NJ). Calcein was purchased from Invitrogen (Carlsbad, CA). PEG of molecular mass 8000 Da (PEG8000) was purchased from Sigma-Aldrich (St. Louis, MO). All materials were used as delivered.

GUVs and micropipettes

GUVs, with and without dyes, were produced by the electroformation method (25) in a production chamber containing 200 mM sucrose solution. For GUVs with dyes, lipids of a selected composition and 0.5% molar ratio of NBD-PC or Rh-DOPE were codissolved in 1:1 (v/v) TFE and chloroform. For GUVs without dyes, the same lipid composition without the dye lipid was used. The lipid solution (~0.07 mg lipid) was deposited onto two indium-tin-oxide (ITO)-coated glass coverslips. After the solution was dried under vacuum, an o-ring was sandwiched between two ITO slips and the gap was filled with 200 mM sucrose solution. Then, 3 V AC at 10 Hz was applied between the two ITO electrodes for 1 h. Subsequently, the frequency was adjusted to 5 Hz for 20 min and then 0.5 Hz for 30 min. This electroformation method has been shown to produce giant unilamellar vesicles (25). The vesicle suspension was then gently collected in a glass vial. The vesicles were used within 24 h of production. The osmolality of every solution used in the GUV experiment was measured on a dew-point osmometer (model 5520; Wescor, Logan, UT).

Micropipettes were made with the use of a micropipette puller (P-97; Sutter Instrument, Novato, CA) and refined by a microforge (MF-900; Narishige, East Meadow, NY). Two micropipettes (diameter 8–16 μm) were used to hold and position the GUVs. Each micropipette was held by a motor-driven micromanipulator (MM-188NE; Narishige) and connected to a micrometer-positioned water (or oil) manometer. The latter was used to create suction pressure inside the micropipette (26). Before use, the micropipettes were coated with 1% bovine serum albumin (BSA) to neutralize the charge on the bare glass surface, and then washed extensively with water. Similar treatments were applied to the walls of the observation chamber. All GUV experiments were performed at room temperature (~25°C).

For the second and third examples of mediator-induced lipid interactions, a third pipette (diameter ~15 μm) was used to inject a PEG or TAT solution. The injection micropipette was connected to an electrical microinjector (IM-31; Narishige) driven by compressed gas. A small negative pressure was maintained before and after injection to ensure that no solution in the injection pipette was leaked. The injection was triggered by a foot switch connected to an electrical microinjector set at ~1 kPa. The injection rate was calculated to be 0.015μL/s.

Weak adhesion experiment

For the weak adhesion experiment, we used a method that was first developed by Evans and co-workers (1,16,21–24) using a flaccid GUV against a tensed GUV; however, we applied a slightly different data analysis. To clearly determine the contours of the lipid vesicles, we used GUVs containing a lipid dye. We transferred 10 μL of the SOPC GUV suspension (at 200 mM osmolality) from the production chamber to an observation chamber (500 μL) that contained 220 mM glucose at a pH controlled by 10 mM of buffer (pH 7 by HEPES, pH 6 by KH_2PO_4-NaOH, and pH 5 by citrate). The GUVs rapidly deflated to new, smaller equilibrium volumes. One GUV was aspirated by a micropipette and held with sufficient suction to form a rigid spherical segment outside the pipette. During the adhesion experiment, this tensed GUV was held at the constant suction pressure. A second GUV was aspirated by another micropipette with an initial suction pressure equivalent to ~20 mm water. We then maneuvered the GUV into close proximity to the tensed GUV and allowed the adhesion process to proceed in discrete steps by lowering the suction pressure in the second pipette (Fig. 1). In a reverse process, the adhered GUV was dissociated from the tensed GUV by stepwise increases in suction pressure, so the reversibility of the adhesion process could be evaluated. The entire process was recorded by fluorescence imaging with a Nikon coolSNAP HQ2 camera.

Adhesion induced by the transient presence of mediators

We studied induced adhesion by injecting a small amount of mediators between two tensed GUVs within a short time interval. After the injection, mediator molecules that were not bound to the GUVs dispersed in the observation chamber to such a low concentration that no further interaction with the GUVs was detectable. For this experiment, the osmolality of the glucose solution in the observation chamber was kept the same as that of

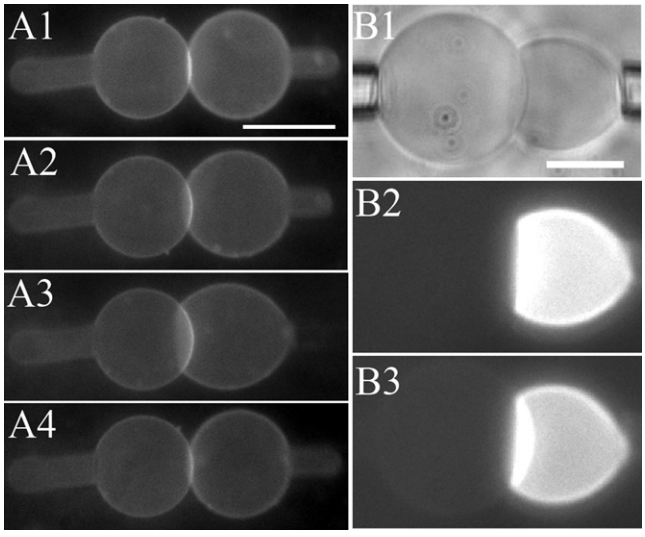

FIGURE 1 (*A*) Fluorescence images of an adhesion process, with SOPC GUVs at pH 5. The right-hand GUV was initially held at a suction pressure ~20 mm water and positioned to contact the tensed GUV on the left-hand side. (*A1*) The suction pressure for the right GUV was lowered to ~3.2 mm to allow adhesion. (*A2* and *A3*) The suction was further lowered to allow more adhesion. (*A4*) The suction pressure was increased to the pressure of *A1*. Scale bar = 50 μm. (*B*) Lipid dye transfer. (*B1*) White-light image of adhered GUVs. (*B2* and *B3*) Lipid dye transfer images at time 66 s and 476 s. Scale bar = 25 μm.

the sucrose solution in the production chamber. Two GUVs were aspirated by two separate micropipettes, each to a membrane tension ~0.7 dyn/cm, and then positioned to slightly contact each other. From a distance of ~200 μm, a small amount of mediator in isotonic solution was injected toward the vicinity of the two contacting GUVs (Fig. 2).

PEG as the mediator. PEG of high molecular weight (e.g., PEG8000) in solution has been shown to induce osmotic depletion attraction between two surfaces in close proximity (2,16). A small amount of 5 wt % PEG8000 solution at pH 7, 6, 5, or 4 (by citrate), adjusted to 200 mM osmolality by glucose and buffer, was injected toward the vicinity of the two contacting GUVs. The injection apparently produced an attractive force between the two GUVs, as a flat contact zone developed between them (Fig. 2). In most cases, once the injection stopped, the GUVs bounced back from the contact and separated. However, for certain lipid compositions (e.g., DOPC/DOPE/cholesterol (2:2:1)), if the injected PEG solution was at pH ~4, the two GUVs remained adhered to each other and we could not separate them by increasing the suction pressure or manipulating the micropipettes. Subsequent dye transfer tests showed that the contact zone developed to hemifusion. Hemifusion did not occur if the injected PEG solution had a pH $>$ 4 or the injected solution contained no PEG. For a lipid composition such as pure DOPC, no hemifusion occurred in any case. Note that to allow the pH effect to work, we set up the experiment with no buffers in the observation chamber to ensure that during the injection the two GUVs would be temporarily surrounded by low pH. If the observation chamber solution was buffered at pH 4, the GUVs were too fragile (i.e., they had a tendency to rupture upon small disturbance) to perform this experiment.

It is important to make clear that the effect of PEG occurred only during the injection. Once the injection stopped, the PEG molecules were dispersed and the bulk effect was negligible. The same experiment was repeated many times. The maximum amount of PEG injected into the observation chamber was equivalent to a concentration of 0.038 wt % PEG. The PEG-induced osmotic depletion attraction between lipid bilayers was previously measured by Kuhl et al. (2) Below a 1 wt % PEG concentration, there was no detectable effect of osmotic depletion attraction. Indeed, we found that there was no attraction between two GUVs after the injection stopped. Therefore, in our experiment the attractive force between the two GUVs was a transient effect during the injection.

TAT as mediators. The experimental setup used for TAT was the same as that used for the PEG experiment, except that the injected solution was 20 μM TAT in 10 mM HEPES (pH 7) and 190 mM glucose (total osmolality 200 mM). The maximum amount of TAT injected was equivalent to 6 nM when dispersed to the entire observation chamber. At this TAT concentration, no effect on GUVs was detected.

As long as the GUV composition included anionic lipids (e.g., DOPC/DOPG (7:3) or DOPC/DOPE/DOPG/cholesterol (2:2:1:1)), an injection of TAT solution produced a stable contact zone between two GUVs (Fig. 3). The contact zone developed into hemifusion in the case of DOPC/DOPE/DOPG/cholesterol (2:2:1:1), but not in the case of DOPC/DOPG (7:3).

Lipid dye transfer and content mixing experiments. The occurrence of hemifusion was established by a test that showed transfer of lipid dye

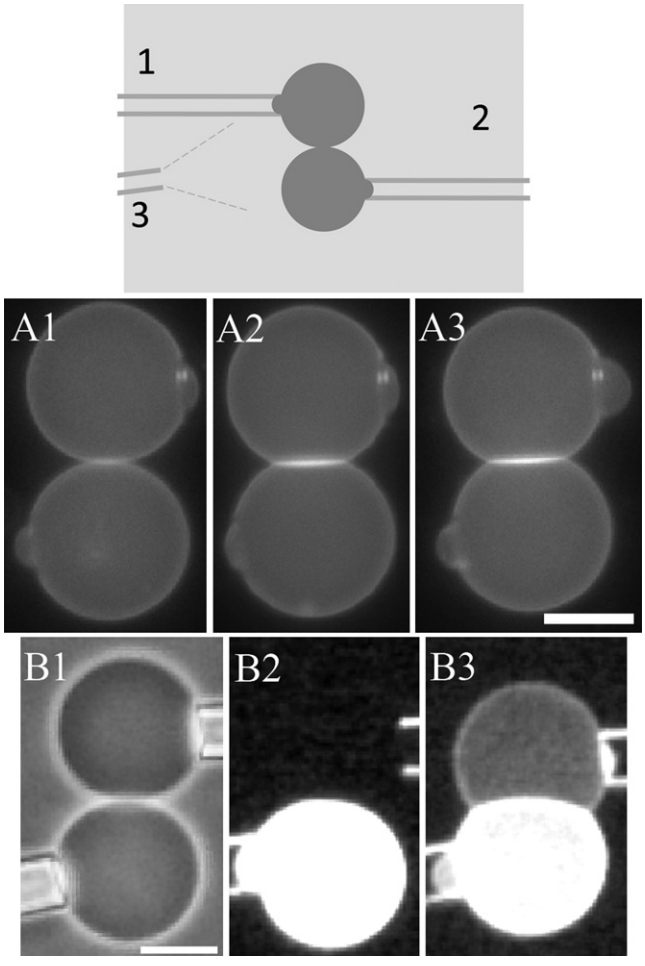

FIGURE 2 (*Top*) Schematic of GUV adhesion induced by a transient injection of mediators. Two GUVs were aspirated by micropipettes 1 and 2. The mediators were injected from pipette 3, ~200 μm away. (*A*) Fluorescence images of GUVs of DOPC/DOPE/cholesterol (2:2:1) induced to hemifusion by PEG at pH 4. (*A1*) Before injection. (*A2*) A contact zone was developed upon injection. (*A3*) Another stable adhesion state at a higher suction pressure. (*B*) Lipid dye transfer. (*B1*) White-light image before injection. (*B2* and *B3*) Lipid dye transfer images at time 0 s and 237 s. Both scale bars = 25 μm.

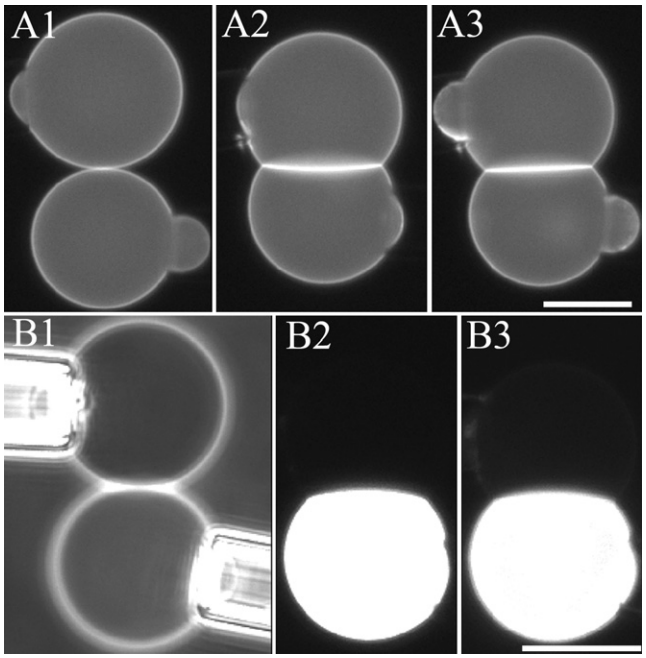

FIGURE 3 GUVs of DOPC/DOPG (7:3) induced to adhere by TAT. (*A*) Fluorescence images (*A1*) before injection and (*A2*) after injection. (*A3*) Another stable adhesion state at a higher suction pressure. (*B*) Lipid dye transfer. (*B1*) White-light image before injection. (*B2* and *B3*) Lipid dye transfer images at time 51 s and 552 s. Both scale bars = 25 μm.

from one GUV to another, and a second test that showed no transfer of aqueous contents between the two GUVs (27). The dye transfer was monitored by the fluorescence images recorded throughout the experiment (Figs. 1–3). One GUV with lipid dye and one GUV without dye were used as a pair. Let I_o and I be the fluorescence intensity per unit area through the originally dyed GUV and the originally undyed GUV, respectively. Assuming that the dye transfer occurred between the outer leaflets of the two hemifused bilayers, one can predict the saturation value of I/I_o to be $1/[2+(A_2/A_1)]$, where A_1 and A_2 are the membrane areas of the originally dyed GUV and undyed GUV, respectively (28,29). The dye transfer curves were plotted as the ratio of the experimental $(I/I_o)_{expt}$ over the theoretical value $(I/I_o)_{theo} = 1/[2+(A_2/A_1)]$, as shown in Fig. 4. For example, when GUVs of composition DOPC/DOPE/cholesterol (2:2:1) were induced to adhere by PEG at pH 4, the experimental value of $(I/I_o)_{expt}$ reached the theoretical value (Fig. 4), indicating a dye transfer between the outer leaflets only. In contrast, there were only very small amounts of dye transfer when two GUVs adhered but did not hemifuse (Fig. 4).

To determine whether content mixing occurred between the aqueous compartments of the two contacting GUVs, we included 8 μM calcein (which is below the quenching concentration) in the content of one GUV (with lipid dye). In all cases, we detected no transfer of dye between the vesicle contents (not shown). Inspection of both the content dye leakage and the GUV phase contrast (sucrose inside versus glucose outside) showed that none of the GUVs were permeabilized during the experiments. Two lipid vesicles were in a hemifusion state when the outer leaflets of the two bilayers merged, but the inner leaflets and aqueous compartments remained separated (27).

RESULTS

Measurement of the free energy of adhesion

For the free-energy measurement, we used two GUVs both containing a lipid dye. As discussed below, the contours of the GUVs must be clearly imaged for the purpose of analysis. After a stable contact zone was established, the suction pressure was increased stepwise to reach a series of new stable or metastable states of adhesion, so that each adhesion state was measured multiple times at different suction pressures.

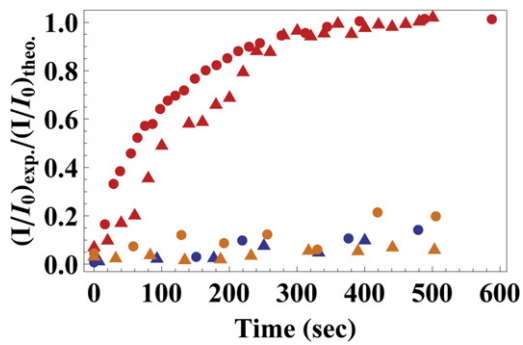

FIGURE 4 Lipid dye transfer between two adhered GUVs. The transferred fluorescence intensity I is divided by the remaining fluorescence intensity I_o as a function of time. The ordinate is the ratio of the experimental value $(I/I_o)_{expt}$ over the theoretical value $(I/I_o)_{theo} = 1/[2+(A_2/A_1)]$. For clarity, only two examples are shown for each of three cases. Red symbols: GUVs of DOPC/DOPE/cholesterol (2:2:1) induced to hemifuse by PEG at pH 4. Blue symbols: SOPC GUVs adhered at pH 5. Brown symbols: GUVs of DOPC/DOPG (7:3) induced to adhere by TAT.

Data analysis for weak adhesion

We use the thermodynamic principle that when a system is in equilibrium, its free energy is minimal with respect to perturbations. This method is applicable to any equilibrium state independently of how the state is reached. Although our method and the method used previously by Evans and Metcalfe (22) are both based on the principle of work and energy, we believe that our method has the advantage of conceptual simplicity. For example, it is straightforward to apply our method to two different adhesion experiments, as we demonstrate below.

The system under consideration is a flaccid GUV that spontaneously adhered to a stationary tensed GUV (Fig. 1). Note that the free energy associated with the membrane tension τ is $\int \tau dA$, where A represents the area of the membrane and $\tau = K_a\Delta A/A_o$; K_a is the membrane stretch constant (30), A_0 is the area of unstretched membrane, and $\Delta A + A_0$ is the area of the stretched membrane. The energy change due to a small increase of area δA is $\frac{1}{2}K_a(\Delta A + \delta A)^2/A_o - \frac{1}{2}K_a(\Delta A)^2/A_o = \tau\delta A$.

We assume that the adhered GUV consists of 1), the adhered area on the surface of the stationary tensed GUV of radius r; 2), a cylindrical part inside the micropipette of radius R_p; and 3), the unadhered part, or the area between the parts 1 and 2, which is spherical with a radius R (Fig. 5 *A*). Note that the sphericalness of the unadhered part is not a condition of equilibrium. Rather, we simply select those equilibrium states in which the unadhered area appears to be spherical. This is done for the purpose of data analysis, for which the area of the GUV must be measured. We realize that this is not exact. The uncertainty

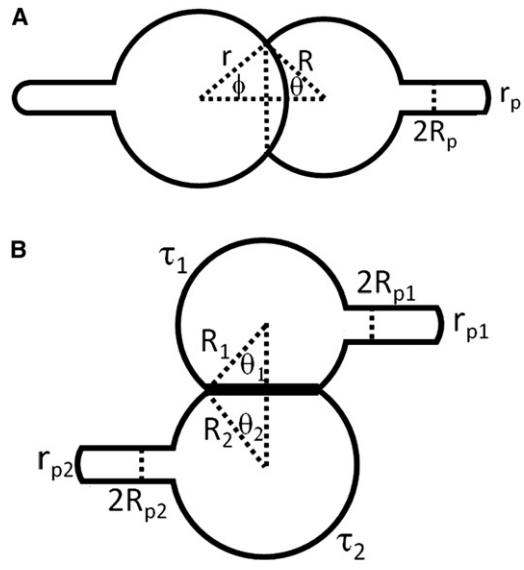

FIGURE 5 Geometry of two adhered GUVs. (*A*) Weak adhesion between a flaccid GUV (*right*) and a tensed GUV (*left*). (*B*) Strong adhesion between two tensed GUVs.

of this area estimate is the main source of error for this method.

The energy variation δF due to a perturbation consists of three terms, and the total is zero at equilibrium:

$$\delta F = \tau\delta A + \gamma 2\pi r^2 sin\phi\delta\phi - (\Delta P)\pi R_p^2\delta L = 0 \quad (1)$$

The first term is the tension term due the area change δA by perturbation. The second term is due to the change of the adhesion area by perturbation, with γ defined as the adhesion energy per unit area. The third term is the work done by the suction pressure ΔP, defined as the atmospheric pressure minus the pressure inside the micropipette, with δL defined as the increase of the protrusion length inside the micropipette due to the perturbation. We did not include the bending energy because it is orders of magnitude smaller than the tension energy (16,30). τ is obtained from the Laplace equations (31): $2\tau(1/r_p - 1/R) = \Delta P$, where r_p is the radius of the curvature of the protrusion cap inside the micropipette. The value of r_p was measured and was not necessarily equal to R_p.

A perturbation causes variations in six variables—δR, $\delta\theta$, $\delta\phi$, δL, δA, and $\delta\tau$ (where the angles θ and ϕ are defined in Fig. 5 *A*)—subject to the five constraints listed below. (We considered but did not include the variable δr_p, which makes small contributions to the volume and area variations. We found that inclusion of the variable δr_p changed the free energy γ by <3%, which is insignificant in view of the larger errors in measurements.)

(i) The volume within the GUV remains constant, or there is no influx or outflux of water. This condition has been well-established in GUV aspiration experiments (26,30–33):

$$\pi R^3\left[\frac{2}{3} + cos\theta - \frac{1}{3}cos^3\theta\right] - \pi r^3\left[\frac{2}{3} - cos\phi + \frac{1}{3}cos^3\phi\right] + \pi R_p^2 L = const \quad (2)$$

(ii) The total area of the GUV consists of three parts as stated above:

$$\delta A = \delta\left[2\pi R^2(1 + cos\theta) + 2\pi r^2(1 - cos\phi) + 2\pi R_p L\right] \quad (3)$$

(iii) The contact areas of the two GUVs are the same:

$$Rsin\theta = rsin\phi \quad (4)$$

(iv) The tension-area relation is:

$$\delta\tau = K_a\frac{\delta A}{A} \quad (5)$$

(v) The Laplace equation is $P_{GUV} - P_{atm} = 2\tau/R = const.$ Because there is no change in the pressure, we have

$$\frac{\delta\tau}{\tau} = \frac{\delta R}{R} \quad (6)$$

We used Eqs. 2–6 to reduce the number of independent variation variables from 6 to 1. Thus, Eq. 1 is solvable for the unknown quantity γ, the adhesion free energy per unit area.

Our method allows variations of all the variables of the system under consideration, except for the constant volume in each GUV. The constant volume of a GUV is a well-established condition during the aspiration process. The developers of the aspiration method (23), as well as results from our own experiments (26,32,33), have shown that as long as the osmotic balance is maintained between the inside and outside of a GUV, the volume of the GUV will remain constant. For comparison, the previous method of Evans and Metcalfe (22) assumes that the area, tension, and volume do not change during perturbation. In addition, to simplify the calculation for the geometric factor, we chose only those equilibrium states in which the unattached part of the GUV was spherical. The main source of errors when a GUV is used to calculate the energy is always the geometric factor (22).

Data analysis for strong adhesion

The equilibrium states of a strong adhesion are shown in Figs. 2 and 3, i.e., two spherical GUVs, labeled 1 and 2, with a flat contact zone in between (Fig. 5 *B*). The sphericalness of the unattached parts of the GUVs and the flatness of the contact zone are not the condition of equilibrium. We select pairs of GUVs of approximately the same size, aspirate each pair by the same suction pressure, and select the cases that have flat contact zones. We adjust the positions of the micropipettes until the unattached parts of both GUVs appear to be spherical. This is strictly for the purpose of measuring the membrane area. Upon perturbation, the free-energy variation δF consists of the tension terms, the adhesion terms, and the work terms by suction for both GUVs:

$$\delta F = \tau_1\delta A_1 + \tau_2\delta A_2 + \gamma\cdot\delta\left(\pi R_1^2 sin^2\theta_1\right) - (\Delta P_1)\pi R_{p1}^2\delta L_1 - (\Delta P_2)\pi R_{p2}^2\delta L_2 = 0 \quad (7)$$

with $2\tau_1(1/r_{p1} - 1/R_1) = \Delta P_1$, and $2\tau_2(1/r_{p2} - 1/R_2) = \Delta P_2$,

A perturbation causes variations in 10 variables—δR_1, δR_2, $\delta\theta_1$, $\delta\theta_2$, δL_1, δL_2, δA_1, δA_2, $\delta\tau_1$, and $\delta\tau_2$ (Fig. 5 *B*)—subject to nine constraints. (Again, we did not include δr_{p1} and δr_{p2}, for the reasons noted above.)

(i) The volume of each GUV remains constant:

$$\pi R_1^3\left[\frac{2}{3} + cos\theta_1 - \frac{1}{3}cos^3\theta_1\right] + \pi R_{p1}^2 L_1 = const \quad (8)$$

$$\pi R_2^3\left[\frac{2}{3} + cos\theta_2 - \frac{1}{3}cos^3\theta_2\right] + \pi R_{p2}^2 L_2 = const \quad (9)$$

(ii) The total area of each GUV consists of the spherical part, the contact zone, and the protrusion inside the micropipette:

$$\delta A_1 = \delta\left[2\pi R_1^2(1+cos\theta_1) + \pi R_1^2 sin^2\theta_1 + 2\pi R_{p1}L_1\right] \quad (10)$$

$$\delta A_2 = \delta\left[2\pi R_2^2(1+cos\theta_2) + \pi R_2^2 sin^2\theta_2 + 2\pi R_{p2}L_2\right] \quad (11)$$

(iii) The contact areas of the two GUVs are the same:

$$R_1 sin\theta_1 = R_2 sin\theta_2 \quad (12)$$

(iv) The tension-area relations are:

$$\delta\tau_1 = K_a\frac{\delta A_1}{A_1} \quad (13)$$

$$\delta\tau_2 = K_a\frac{\delta A_2}{A_2} \quad (14)$$

(v) The Laplace equation is $P_{GUV} - P_{atm} = 2\tau/R = const.$ Because there is no change in the pressures, we have

$$\frac{\delta\tau_1}{\tau_1} = \frac{\delta R_1}{R_1} \quad (15)$$

$$\frac{\delta\tau_2}{\tau_2} = \frac{\delta R_2}{R_2} \quad (16)$$

Weak adhesion experiment

For lipid vesicle experiments, it is a standard practice to coat the glass surface with BSA to neutralize the surface charge (34). Because BSA in solution can induce osmotic depletion attraction between lipid bilayers (24), we were concerned about the possibility that the coated BSA might, perhaps in a pH-dependent manner, redissolve into the solution. Therefore, we measured the BSA spectrum (35) of the solution taken from the observation chamber at different pH values. In all cases, we found that the glass-coated BSA did not redissolve into the solution.

Spontaneous adhesion between lipid vesicles can be seen in the vesicle suspension. In SOPC vesicles, we did not detect spontaneous adhesion at pH values 6 and 7 (Fig. 6). However, at pH $\leq$5, vesicles spontaneously adhered to each other in pairs or in multiples (Fig. 6). We observed the same adhesion phenomena by adding acid to achieve pH 5 without buffers. Of importance, the adhesion was reversible. As shown in Fig. 1, the adhesion of the flaccid GUV took place as the suction pressure was decreased. At any step, if the suction pressure was increased, the GUV reversibly detached and recovered the previous states. Because the system was in equilibrium at each suction pressure, the energies measured at different suction pressures were very close (Fig. 7).

The pH-induced adhesion did not produce hemifusion in any of the lipid compositions we tested, including pure SOPC, SOPC/SOPE (4:1), and SOPC/cholesterol (4:1). The energies of adhesion for these lipid compositions at pH 5 are shown in Table 1. There were small variations of adhesion energy with the lipid compositions. The very large standard deviations (~50%) were due to the very small suction pressures used (~0.5–2.5 mm water). The stability of the water manometer is ~0.2 mm.

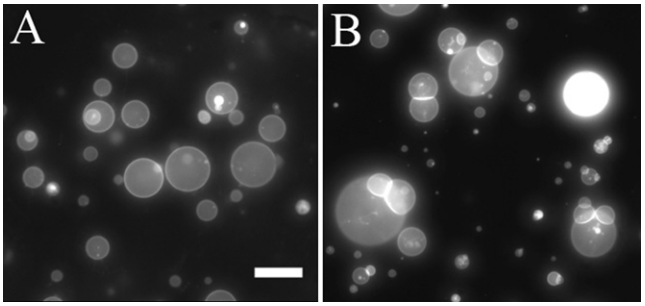

FIGURE 6 GUVs of SOPC spontaneously aggregated at pH 5 (*right*), but did not aggregate at pH 7 (*left*). Scale bar = 50 μm.

Strong adhesion experiment

We induced strong adhesion by introducing mediators between two GUVs for a short period of time (<200 s for PEG and ~5 s for TAT). The mediator molecules that did not bind to the GUVs during that time were all dispersed to negligible concentrations. The PEG-induced attraction created a temporary contact zone between two GUVs. As soon as the PEG injection stopped, the two GUVs detached from each other unless a hemifusion occurred. Hemifusion never occurred with GUVs of pure DOPC. In contrast, between two GUVs of DOPC/DOPE/cholesterol (2:2:1),

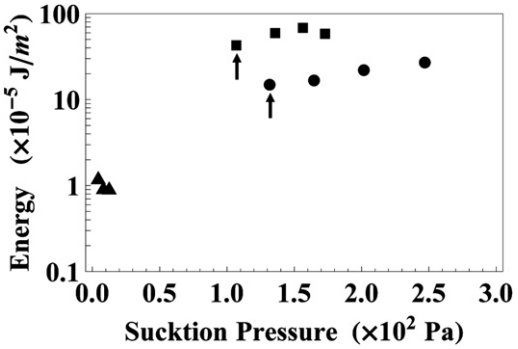

FIGURE 7 Energy of adhesion measured at different suction pressures. For clarity, only one example is shown for each of three types of adhesion. For each adhesion in equilibrium (indicated by *arrows*), a series of stable or metastable states were created by increasing suction pressures. The free energy of adhesion was calculated for each stable state. Squares: GUVs of DOPC/DOPG (7:3) induced to adhere by TAT. Circles: GUVs of DOPC/DOPE/cholesterol (2:2:1) induced to hemifuse by PEG at pH 4. Triangles: SOPC GUVs adhered at pH 5 (all three points were in equilibrium).

TABLE 1 Free energy of adhesion

	Average ($\times 10^{-5}$ J/m^2)	Standard deviation	Number of runs
Adhesion at pH 5			
SOPC	−1.72	0.90	6
SOPC/SOPE 4:1	−1.04	0.47	6
SOPC/Chol 4:1	−1.81	0.72	7
Hemifusion by PEG at pH 4			
DOPC/DOPE/Chol 2:2:1	−13.20	1.47	3
Adhesion by TAT at pH 7			
DOPC/DOPG 7:3	−50.08	8.32	5
Hemifusion by TAT at pH 7			
DOPC/DOPE/Chol/DOPG 2:2:1:1	−51.77	7.87	3

hemifusion occurred at a random time during the injection of PEG solution, indicating a stochastic process. The observation that cone-shaped lipids, such as PE and cholesterol, promoted hemifusion was expected (36). However, hemifusion occurred only when the injected PEG solution was pH 4, and not at any higher pH. Whether this is related to the low-pH-induced adhesion observed with SOPC remains to be investigated.

The TAT injection to anionic GUVs always created a stable contact zone. There was no hemifusion in the case of DOPC/DOPG (7:3). In the case of DOPC/DOPE/DOPG/cholesterol (2:2:1:1), the contact zone developed into hemifusion. We measured the energy of adhesion at the initial equilibrium state and also at a series of stable or metastable states created by an increase in suction pressure (Fig. 7). In the cases of hemifusion and strong adhesion by TAT, increasing suction pressure reduced the contact zone, which required a small area of strongly adhered bilayers or hemifused bilayers reversed to two separate bilayers. It is possible that the small dependence of γ on the suction pressure (Fig. 7) reflected the incomplete reversibility during the experimental time. The average values given in Table 1 include only the measurements for the initial equilibrium states.

DISCUSSION

It is clear from these examples that there are many molecular mediators that can cause interactions between lipid bilayers. The adhesion of SOPC vesicles was readily observable at pH < 5 (Fig. 6). The same adhesion phenomenon was observed regardless of whether the low pH was achieved by a buffer or by addition of acid to the solution. In a previous study, Evans and Needham (16) measured the adhesion between two SOPC GUVs in 0.1 M NaCl (pH 7.0 buffer) and obtained an adhesion energy of -1.3×10^{-5}J/m^2, which is comparable to our $\gamma = -(1.72 \pm 0.90)10^{-5}$J/m^2 at pH 5 without salt. Perhaps H^+ and Na^+ ions have the same effect on SOPC; however, the exact mechanism that causes the bilayer adhesion is not clear.

On the other hand, it is known that adhesion occurs between anionic bilayers cross-bridged by multivalent cations, such as La^{+3} (37) and Eu^{+3} (38). We tested several cationic peptides for this effect: magainin, which has +6 (including the N-terminus) and −1 charges in 23 amino acids; melittin, which has +6 charges in 26 amino acids; and TAT, which has +8 charges in 13 amino acids. Only TAT could induce adhesion between anionic lipids. Lastly, although we expected PEG to produce osmotic depletion attraction between bilayers, we were surprised to find that PEG at pH 4 (but not at any higher pH) induced hemifusion in PE/cholesterol-containing lipids.

How should such adhesions be characterized? We suggest that the most important characteristic is the free energy of adhesion, and propose a method that can successfully measure this property for all of the examples discussed above. Our method can measure a wide range of adhesion energies, at least from -1×10^{-5}J/m^2 to -50×10^{-5}J/m^2. In fact, we do not expect an instrumental limit for large values of adhesion energy. It is clear that cross-bridging by TAT dominated the adhesion energy whether hemifusion occurred or not. Thus, TAT-induced adhesion or hemifusion had a γ -value of $\sim -50 \times 10^{-5}$J/m^2 whereas γ for hemifusion induced by PEG was $\sim -13 \times 10^{-5}$J/m^2. These values can be compared with SOPC adhesion $\gamma = -12 \times 10^{-5}$J/m^2 under the effect of constant osmotic depletion force induced by 9.3 g/100 cm^3 dextran (MW 36500) measured by Evans and Needham (16).

The methods we have discussed here are relevant to some crucial questions in the field of membrane fusion research. Membrane fusion is a complicated yet ubiquitous process that occurs constantly in eukaryotic cells. Active research on this subject over the last two decades has clarified the roles of various fusion proteins (39–45). There is now a converging view that the formation of fusion protein complexes (13,40,43,46) exerts a force that pulls two membranes into close proximity. The fusion proteins are anchored to the fusing membranes via a transmembrane domain or a fusion peptide. However, exactly how the proteins manipulate the two lipid bilayers to merge remains unclear (47,48). Three questions relevant to our discussion are: 1), How do the two lipid bilayers come into contact? 2), What causes the transition to hemifusion? 3), Is the hemifusion intermediate state a free-energy barrier, as is often suggested (7–12)?

Despite the fact that cell membranes are generally covered by carbohydrates glycosylated to lipids and proteins, it is commonly believed that one of the key steps during membrane fusion involves the creation of a protein-denuded contact zone in each of the two fusing membranes so as to allow bilayer-bilayer contact and merger (43). However, since the bulky fusion-protein complexes are between the two membranes, the cause of the bilayer-bilayer contact has been a major puzzle (43,46–48). Could it be that fusion proteins simply need

to pin two bilayers together long enough and the bilayers do the rest spontaneously, or do the fusion proteins play an active role in directing the contact and merger between two bilayers (46)? Perhaps mediated adhesion between bilayers, as discussed here, is a factor in membrane fusion, particularly at low pH.

It is now believed that most, if not all, biological membrane fusion proceeds through a hemifusion intermediate (27). The structure of this fusion intermediate, which is termed the stalk, has been confirmed by x-ray diffraction (49). In fact, the stalk structure was theoretically predicted (7) almost 20 years before it was confirmed by experiment (49). However, there is wide theoretical disagreement about the free-energy level of hemifusion (7–12). This is not merely a theoretical curiosity. Knowing the energy levels of the intermediate states would help us understand the actions of fusion proteins. The methods demonstrated here provide a means of systematic measurements to resolve the energy issue for the intermediate states of lipid transformation during membrane fusion.

This work was supported by the National Institutes of Health (grant GM55203) and the Robert A. Welch Foundation (grant C-0991).

REFERENCES

1. Evans, E., and M. Metcalfe. 1984. Free energy potential for aggregation of giant, neutral lipid bilayer vesicles by Van der Waals attraction. *Biophys. J.* 46:423–426.
2. Kuhl, T., Y. Guo, …, S. W. Hui. 1996. Direct measurement of polyethylene glycol induced depletion attraction between lipid bilayers. *Langmuir.* 12:3003–3014.
3. Rand, R. P., and V. A. Parsegian. 1989. Hydration forces between phospholipid bilayers. *Biochim. Biophys. Acta.* 988:351–376.
4. Helfrich, W. 1978. Steric interaction of fluid membranes in multilayer systems. *Z. Naturforsch. C.* 33a:305–315.
5. Ding, L., T. M. Weiss, …, H. W. Huang. 2005. Distorted hexagonal phase studied by neutron diffraction: lipid components demixed in a bent monolayer. *Langmuir.* 21:203–210.
6. Wang, W., L. Yang, and H. W. Huang. 2007. Evidence of cholesterol accumulated in high curvature regions: implication to the curvature elastic energy for lipid mixtures. *Biophys. J.* 92:2819–2830.
7. Markin, V. S., M. M. Kozlov, and V. L. Borovjagin. 1984. On the theory of membrane fusion. The stalk mechanism. *Gen. Physiol. Biophys.* 3:361–377.
8. Siegel, D. P. 1993. Energetics of intermediates in membrane fusion: comparison of stalk and inverted micellar intermediate mechanisms. *Biophys. J.* 65:2124–2140.
9. Kuzmin, P. I., J. Zimmerberg, …, F. S. Cohen. 2001. A quantitative model for membrane fusion based on low-energy intermediates. *Proc. Natl. Acad. Sci. USA.* 98:7235–7240.
10. Kozlovsky, Y., and M. M. Kozlov. 2002. Stalk model of membrane fusion: solution of energy crisis. *Biophys. J.* 82:882–895.
11. Markin, V. S., and J. P. Albanesi. 2002. Membrane fusion: stalk model revisited. *Biophys. J.* 82:693–712.
12. Lentz, B. R., D. P. Siegel, and V. Malinin. 2002. Filling potholes on the path to fusion pores. *Biophys. J.* 82:555–557.
13. Hernandez, L. D., L. R. Hoffman, …, J. M. White. 1996. Virus-cell and cell-cell fusion. *Annu. Rev. Cell Dev. Biol.* 12:627–661.
14. Chernomordik, L. V., E. Leikina, …, J. Zimmerberg. 1997. An early stage of membrane fusion mediated by the low pH conformation of influenza hemagglutinin depends upon membrane lipids. *J. Cell Biol.* 136:81–93.
15. Zhou, Y., and R. M. Raphael. 2007. Solution pH alters mechanical and electrical properties of phosphatidylcholine membranes: relation between interfacial electrostatics, intramembrane potential, and bending elasticity. *Biophys. J.* 92:2451–2462.
16. Evans, E., and D. Needham. 1988. Attraction between lipid bilayer membranes in concentrated solutions of nonadsorbing polymers: comparison of mean-field theory with measurements of adhesion energy. *Macromolecules.* 21:1822–1831.
17. Console, S., C. Marty, …, K. Ballmer-Hofer. 2003. Antennapedia and HIV transactivator of transcription (TAT) "protein transduction domains" promote endocytosis of high molecular weight cargo upon binding to cell surface glycosaminoglycans. *J. Biol. Chem.* 278:35109–35114.
18. Richard, J. P., K. Melikov, …, L. V. Chernomordik. 2005. Cellular uptake of unconjugated TAT peptide involves clathrin-dependent endocytosis and heparan sulfate receptors. *J. Biol. Chem.* 280:15300–15306.
19. Wadia, J. S., R. V. Stan, and S. F. Dowdy. 2004. Transducible TAT-HA fusogenic peptide enhances escape of TAT-fusion proteins after lipid raft macropinocytosis. *Nat. Med.* 10:310–315.
20. Yang, S. T., E. Zaitseva, …, K. Melikov. 2010. Cell-penetrating peptide induces leaky fusion of liposomes containing late endosome-specific anionic lipid. *Biophys. J.* 99:2525–2533.
21. Evans, E. A. 1980. Analysis of adhesion of large vesicles to surfaces. *Biophys. J.* 31:425–431.
22. Evans, E., and M. Metcalfe. 1984. Free energy potential for aggregation of mixed phosphatidylcholine/phosphatidylserine lipid vesicles in glucose polymer (dextran) solutions. *Biophys. J.* 45:715–720.
23. Evans, E., and D. Needham. 1987. Physical properties of surfactant bilayer membranes: thermal transitions, elasticity, rigidity, cohesion, and colloidal interactions. *J. Phys. Chem.* 91:4219–4228.
24. Evans, E., D. Needham, and J. Janzen. 1987. Nonspecific adhesion of phospholipid bilayer membranes in solutions of plasma proteins: measurement of free energy potentials and theoretical concepts. *In* Proteins at Interfaces. J. Brash and T. Horbett, editors. American Chemical Society, Washington, DC. 88–102.
25. Angelova, M. I. 2000. Liposome electroformation. *In* Giant Vesicles. P. L. Luisi and P. Walde, editors. John Wiley & Sons, Chichester. 27–36.
26. Sun, Y., C. C. Lee, …, H. W. Huang. 2008. The bound states of amphipathic drugs in lipid bilayers: study of curcumin. *Biophys. J.* 95: 2318–2324.
27. Chernomordik, L. V., and M. M. Kozlov. 2008. Mechanics of membrane fusion. *Nat. Struct. Mol. Biol.* 15:675–683.
28. Heuvingh, J., F. Pincet, and S. Cribier. 2004. Hemifusion and fusion of giant vesicles induced by reduction of inter-membrane distance. *Eur. Phys. J. E. Soft Matter.* 14:269–276.
29. Rodriguez, N., J. Heuvingh, …, S. Cribier. 2005. Indirect evidence of submicroscopic pores in giant unilamellar [correction of unilamelar] vesicles. *Biochim. Biophys. Acta.* 1724:281–287.
30. Rawicz, W., K. C. Olbrich, …, E. Evans. 2000. Effect of chain length and unsaturation on elasticity of lipid bilayers. *Biophys. J.* 79:328–339.
31. Kwok, R., and E. Evans. 1981. Thermoelasticity of large lecithin bilayer vesicles. *Biophys. J.* 35:637–652.
32. Sun, Y., W. C. Hung, …, H. W. Huang. 2009. Interaction of tea catechin (−)-epigallocatechin gallate with lipid bilayers. *Biophys. J.* 96:1026–1035.
33. Sun, Y., C. C. Lee, …, H. W. Huang. 2010. Kinetic process of beta-amyloid formation via membrane binding. *Biophys. J.* 99:544–552.
34. Zhelev, D. V., and D. Needham. 1993. Tension-stabilized pores in giant vesicles: determination of pore size and pore line tension. *Biochim. Biophys. Acta.* 1147:89–104.

35. Glazer, A. N., and H. A. McKENZIE. 1963. The denaturation of proteins. IV. Conalbumin and iron(III)-conalbumin in urea solution. *Biochim. Biophys. Acta.* 71:109–123.

36. Chernomordik, L., A. Chanturiya, …, J. Zimmerberg. 1995. The hemifusion intermediate and its conversion to complete fusion: regulation by membrane composition. *Biophys. J.* 69:922–929.

37. Tanaka, T., and M. Yamazaki. 2004. Membrane fusion of giant unilamellar vesicles of neutral phospholipid membranes induced by La^{3+}. *Langmuir.* 20:5160–5164.

38. Haluska, C. K., K. A. Riske, …, R. Dimova. 2006. Time scales of membrane fusion revealed by direct imaging of vesicle fusion with high temporal resolution. *Proc. Natl. Acad. Sci. USA.* 103:15841–15846.

39. Söllner, T., S. W. Whiteheart, …, J. E. Rothman. 1993. SNAP receptors implicated in vesicle targeting and fusion. *Nature.* 362:318–324.

40. Südhof, T. C., and J. E. Rothman. 2009. Membrane fusion: grappling with SNARE and SM proteins. *Science.* 323:474–477.

41. Rizo, J., and C. Rosenmund. 2008. Synaptic vesicle fusion. *Nat. Struct. Mol. Biol.* 15:665–674.

42. Wickner, W., and R. Schekman. 2008. Membrane fusion. *Nat. Struct. Mol. Biol.* 15:658–664.

43. Martens, S., and H. T. McMahon. 2008. Mechanisms of membrane fusion: disparate players and common principles. *Nat. Rev. Mol. Cell Biol.* 9:543–556.

44. Giraudo, C. G., A. Garcia-Diaz, …, J. E. Rothman. 2009. Alternative zippering as an on-off switch for SNARE-mediated fusion. *Science.* 323:512–516.

45. Maximov, A., J. Tang, …, T. C. Südhof. 2009. Complexin controls the force transfer from SNARE complexes to membranes in fusion. *Science.* 323:516–521.

46. McNew, J. A., T. Weber, …, J. E. Rothman. 2000. Close is not enough: SNARE-dependent membrane fusion requires an active mechanism that transduces force to membrane anchors. *J. Cell Biol.* 150:105–117.

47. Kozlov, M. M., H. T. McMahon, and L. V. Chernomordik. 2010. Protein-driven membrane stresses in fusion and fission. *Trends Biochem. Sci.* 35:699–706.

48. McMahon, H. T., M. M. Kozlov, and S. Martens. 2010. Membrane curvature in synaptic vesicle fusion and beyond. *Cell.* 140:601–605.

49. Yang, L., and H. W. Huang. 2002. Observation of a membrane fusion intermediate structure. *Science.* 297:1877–1879.